

Bistability in the synchronization of identical neuronsB. R. R. Boaretto^{1,*}, R. C. Budzinski¹, K. L. Rossi¹, C. Manchein², T. L. Prado¹, U. Feudel³ and S. R. Lopes¹¹*Department of Physics, Universidade Federal do Paraná, 81531-980, Curitiba, PR, Brazil*²*Department of Physics, Universidade do Estado de Santa Catarina, 89219-710 Joinville, SC, Brazil*³*Theoretical Physics/Complex Systems, ICBM, Carl von Ossietzky University Oldenburg, 26111 Oldenburg, Germany*

(Received 17 February 2021; accepted 19 July 2021; published 5 August 2021)

We investigate the role of bistability in the synchronization of a network of identical bursting neurons coupled through an generic electrical mean-field scheme. These neurons can exhibit distinct multistable states and, in particular, bistable behavior is observed when their sodium conductance is varied. With this, we consider three different initialization compositions: (i) the whole network is in the same periodic state; (ii) half of the network periodic, half chaotic; (iii) half periodic, and half in a different periodic state. We show that (i) and (ii) reach phase synchronization (PS) for all coupling strengths, while for (iii) small coupling regimes do not induce PS, and instead, there is a coexistence of different frequencies. For stronger coupling, case (iii) synchronizes, but after (i) and (ii). Since PS requires all neurons being in the same state (same frequencies), these different behaviors are governed by transitions between the states. We find that, during these transitions, (ii) and (iii) have transient chimera states and that (iii) has breathing chimeras. By studying the stability of each state, we explain the observed transitions. Therefore, bistability of neurons can play a major role in the synchronization of generic networks, with the simple initialization of the system being capable of drastically changing its asymptotic space.

DOI: [10.1103/PhysRevE.104.024204](https://doi.org/10.1103/PhysRevE.104.024204)**I. INTRODUCTION**

Nonlinear dynamical systems are known to exhibit asymptotic complex dynamical behaviors such as stationary points, limit cycles, quasiperiodicity, and chaoticity [1–3]. In particular, different stable states of a dynamical system can coexist for a given set of parameters, which characterizes the phenomenon of *multistability* [1,4]. This dynamical feature has been studied for several years and it is observed in areas such as physics [5], chemistry [6], climatology [7], and also neuroscience [8,9].

In neuronal systems, the phenomenon of multistability acts at different levels and can be observed both macroscopically and microscopically. For instance, the coexistence of attractors can be associated with different states of the brain, which was proposed as a possible mechanism for memory storage and pattern recognition [8,9]. This coexistence can also mean that a neuron may depict distinct states, with different firing patterns, frequencies, regularity, and chaoticity [1,10–12].

Most of the complexity seen in the brain is directly related to patterns of neuronal activation [13]. When the oscillatory activities of neurons, or neural areas, are temporally correlated, they can be phase synchronized. Phase synchronization (PS) of neurons is of fundamental interest since abnormalities in this process have been related to several brain disorders: while high degrees of synchronization are seen in epileptic seizures [14] and Parkinson's disease [15,16], reduced levels of synchronization between cortical areas are associated with autism [17], and Alzheimer's disease [18].

Here, we study the synchronization dynamics of a network of bursting neurons simulated through the model of Braun *et al.* [19–21]. This model is a modification of the original Hodgkin-Huxley model [22], with thermal effects added to the neuronal activity [23]. It was shown that the neurons' individual dynamics are controlled by their temperature [21,24,25] and by the conductance of their ionic channels [26,27]. When neurons with a periodic dynamics are coupled, a chemical coupling induces chaoticity in the network and a non-monotonic transition to synchronization is observed as the synaptic strength is varied [28]. Besides this, several dynamical features can be observed with this model: while a neuron under a recurrent connection to itself can change the spiking activity by inducing excitatory and inhibitory behavior [11], networks can depict chimera states and chimeralike behaviors when mean-field and distance-dependent couplings are considered [29].

In this paper, we focus on the role of bistability and its effects on the synchronization process. We first show the existence of a parameter region where the neuron exhibits *bistable* behavior, that is, where a neuron initialized with different initial conditions (ICs) can present two different stable states. Using the Lyapunov spectrum, we show that the linear stability of each state is different. Furthermore, we show that one state is more sensitive to noise than the other, and the mean time that the system spends before escape to the other state follows a Kramers law. This can be used to understand the analysis regarding the coupling effect in the network and the transitions to synchronization. After that, we build a network using a generic mean-field electrical coupling and evaluate the role of the bistability observed in individual neurons in the process of synchronization. To do so, we associate a

*brunorafaelrboaretto@gmail.com

geometric phase to the bursting activity of each neuron and use the Kuramoto order parameter to investigate the phase synchronization features that the network can depict.

We show that a network composed of identical neurons in the same periodic state always reaches phase synchronization, with more weakly coupled networks needing more time to reach the phase-synchronized state. After that, to explore the bistability, we construct two mixed networks: one with a periodic and a chaotic state and another with two different periodic states. In the first case, the presence of chaotic state delays the attainment of phase-synchronized state. However, when two periodic states are considered, smaller values of coupling strength are not able to make the network reach the phase synchronized state, and the system depicts two groups with different synchronization features. If the coupling becomes stronger, then the network can reach PS, but always taking longer than the case without bistability in the network. The transition between the states observed when PS is reached can be understood using the stability of each state. In both cases, interesting dynamical phenomena are observed in the transition to phase synchronization, such as *chimera* states and antiphase synchronization. At last, we show that, if the fraction of neurons in the first periodic state is increased, the behavior of the network becomes closer to the case where all neurons are in the same periodic state.

The paper is organized as follows: in Sec. II, we present details of the model, as well as the properties of the bistable regime; in Sec. III, we introduce the properties of the network as well as the tools to evaluate PS; in Sec. IV, we show the synchronization results considering different network compositions; in Sec. V, we present our conclusions.

II. NEURON MODEL

The neural behavior is simulated through the Hodgkin-Huxley-type thermally sensitive model proposed by Braun *et al.* [20,21,30,31], in which the neuron's membrane potential is given by

$$C_M \frac{dV}{dt} = -I_d - I_r - I_{sd} - I_{sr} - I_l + I_{ext}, \quad (1)$$

where C_M is the membrane capacitance; I_d and I_r represent simplified depolarizing and repolarizing Hodgkin-Huxley currents for action potentials with fast ionic kinetics according to the classical sodium (Na^+) and potassium (K^+) currents, respectively [22]. I_{sd} and I_{sr} are subthreshold depolarization and repolarization currents, respectively, which can be associated with potential-dependent calcium (Ca^{2+}) currents [32]. I_l represents the leakage current which considers the contribution of the nongated channels. The ionic currents are expressed by

$$I_\mu = \rho(T)g_\mu a_\mu (V - E_\mu), \quad \mu = d, r, sd, sr, \quad (2)$$

$$I_l = g_l (V - E_l), \quad (3)$$

with $\rho(T)$ a temperature-dependent scale factor given by $\rho(T) = 1.3^{(T-T_0)/\tau_0}$, g_μ the maximum conductance, and E_μ the reversal potential of each current. The activation term a_μ is associated to the probability of a channel being open.

TABLE I. Parameter values of the neural model.

Membrane Capacitance	$C_M = 1\mu\text{F}/\text{cm}^2$
Maximum Conductances (mS/cm^2)	$g_r = 2.0$
	$g_{sd} = 0.25$
	$g_{sr} = 0.4$
Characteristic Times (ms)	$g_l = 0.1$
	$\tau_d = 0.05$
	$\tau_r = 2.0$
	$\tau_{sd} = 10$
Reversal Potentials (mV)	$\tau_{sr} = 20$
	$E_d = 50$
	$E_r = -90$
	$E_{sd} = 50$
	$E_{sr} = -90$
	$E_l = -60$
	$V_{0d} = -25$
$V_{0r} = -25$	
Temperature Parameters	$V_{0sd} = -40$
	$T_0 = 25^\circ\text{C}$
	$T = 13^\circ\text{C}$
Other Parameters	$\tau_0 = 10^\circ\text{C}$
	$s_d = 0.25 \text{ mV}^{-1}$
	$s_r = 0.25 \text{ mV}^{-1}$
	$s_{sd} = 0.09 \text{ mV}^{-1}$
	$\eta = 0.012 \text{ cm}^2/\mu\text{A}$
	$\gamma = 0.17$

The temporal evolution of each activation term follows the differential equations

$$\frac{da_\mu}{dt} = \frac{\phi(T)}{\tau_\mu} (a_{\mu,\infty} - a_\mu), \quad \mu = d, r, sd, \quad (4)$$

$$\frac{da_{sr}}{dt} = \frac{\phi(T)}{\tau_{sr}} (-\eta I_{sd} - \gamma a_{sr}), \quad (5)$$

where $\phi(T)$ represents another temperature-dependent scale factor given by $\phi(T) = 3^{(T-T_0)/\tau_0}$; τ_μ is a characteristic time corresponding to each activation function [20]. The term η is a factor that relates the mixed Na/Ca current to the increment of intracellular Ca^{2+} , and γ is a rate for Ca^{2+} decrease [32]. The $a_{\mu,\infty}$, for $\mu = d, r, sd$, is defined by

$$a_{\mu,\infty} = \frac{1}{1 + \exp[-s_\mu (V - V_{0\mu})]}, \quad (6)$$

where s_d , s_r , s_{sd} , V_{0d} , V_{0r} , V_{0sd} are constants as defined in Ref. [20].

A. Importance of the individual dynamics

The dynamics of an isolated neuron is depicted in Figs. 1(a) and 1(b), where the parameters of Table I and $g_d = 1.1350$ are used. In this case, the membrane potential V [Fig. 1(a)] displays a set of three spikes followed by a resting period, characterizing a burst. The activation variable a_{sr} [Fig. 1(b)] depicts oscillatory behavior, with its minimum values corresponding to the beginning of the bursts (red dashed lines). With this, we define an Inter-Burst-Interval (IBI) as the time between two consecutive bursts. These are

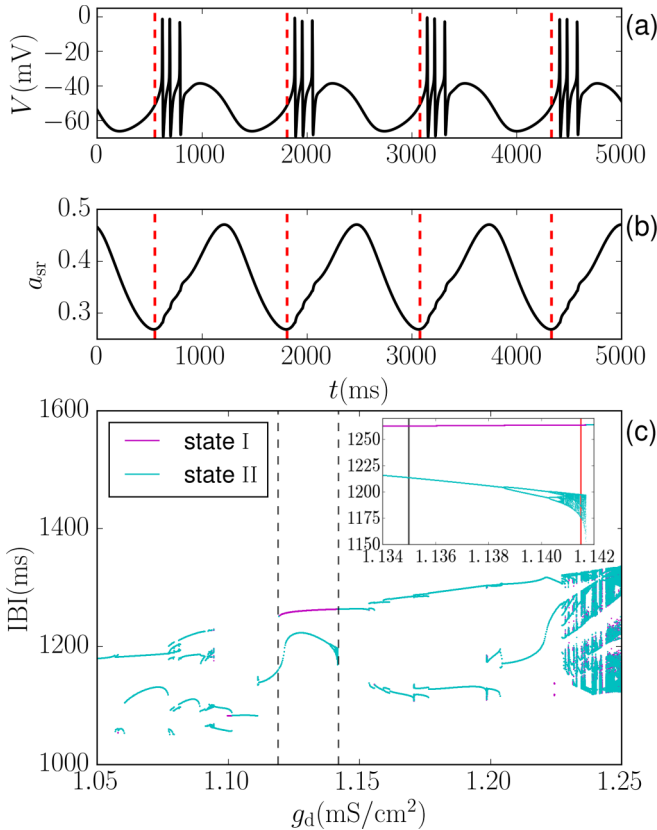


FIG. 1. Membrane potential $V(t)$ (a) and the activation variable $a_{sr}(t)$ (b) as a function of time (with $g_d = 1.1350$). The red dashed lines represent the times where a_{sr} is minimum, and mark the beginning of the bursts, as observed in (a). (c) Bifurcation diagram of the Inter-Burst-Intervals (IBI) as a function of g_d , where two different ICs are shown—cyan and magenta points. The vertical dashed lines delimit the region where bistability is found and state I (magenta) and state II (cyan) are defined. The former is always periodic, while the latter can depict periodic and chaotic behavior depending on the g_d value (see inner panel). The black and red lines in the inner panel indicate the parameters used in this manuscript: $g_d = 1.1350$ and $g_d = 1.1415$.

depicted on panel (c) in a bifurcation diagram of IBI as a function of g_d for two different ICs. Denoting the ICs as $\{V(0), a_d(0), a_r(0), a_{sd}(0), a_{sr}(0)\}$, the magenta dots represent $\{-10, 0, 0, 0, 0.45\}$, named IC-1, and the cyan dots represent $\{-70, 0, 0, 0, 0.45\}$, named IC-2. We focus our attention to the region $1.120 \lesssim g_d \lesssim 1.142$ (between the dashed lines), where the neuron is bistable: IC-1 leads to state I (magenta) and IC-2 leads to state II (cyan). The inner panel exhibits a magnification of the two branches: while state I is always periodic, state II undergoes a sequence of period-doubling bifurcations at $g_d \gtrsim 1.1385$, and finally becomes chaotic. The variation of the sodium conductance in the model can be understood as the increase or decrease of the contribution of the ionic current, which means that a fraction of the voltage-dependent channels (sodium channels, for example) can be blocked or activated by an abnormality that can come from either a disease or a medication drug [33,34].

To study the bistable behavior of the neuron we select two conductances values $g_d = 1.1350$ (before the period-

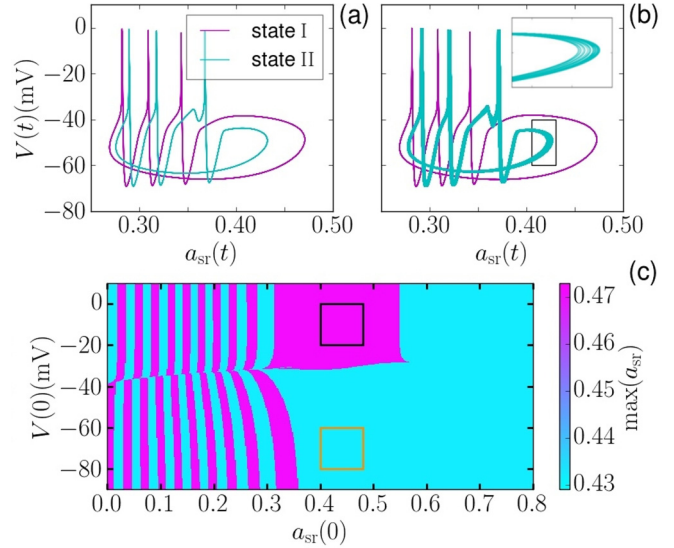


FIG. 2. Two-dimensional projection $V(t) \times a_{sr}(t)$ of the system's phase portrait, (a) where two periodic states are observed with $g_d = 1.1350$, (b) a periodic (magenta) and chaotic (cyan) states are noticed with $g_d = 1.1415$. Each color corresponds to a distinct IC: magenta (cyan) line with IC-1 (IC-2). (c) Maximum values of a_{sr} as a function of $V(t = 0)$ and $a_{sr}(t = 0)$ for $a_d(0) = a_r(0) = a_{sd}(0) = 0$ using $g_d = 1.1350$. The black and orange rectangles delimit the values of ICs that we use to obtain neurons initialized in each state.

doubling, black line) and $g_d = 1.1415$ (after the period-doubling, red line). Figures 2(a) and 2(b) depict the evolution of a two-dimensional projection of the phase portrait of the system into the space spanned by $V(t)$ and $a_{sr}(t)$ where the different colors refers to each IC. In Fig. 2(a) ($g_d = 1.1350$) there is a clear difference between the two states that is explicit in the amplitude of a_{sr} since the state I $\max(a_{sr}) \approx 0.47$ and the state II $\max(a_{sr}) \approx 0.43$. In Fig. 2(b) ($g_d = 1.1415$), one can observe that state II depicts a greater thickness, indicating chaotic motion. The inner panel exhibits a magnification of the chaotic orbit, showing a projection of the chaotic attractor [2]. To numerically find which ICs lead to each state, we set different ICs $\{V(0), 0, 0, 0, a_{sr}(0)\}$ and calculate the maximum values of the neurons' a_{sr} variable, using $g_d = 1.1350$. Figure 2(c) depicts this maximum in color tones from cyan to magenta as a function of $V(0)$ and $a_{sr}(0)$. It therefore corresponds to a two-dimensional cross section of the neuron's basin of attraction since each state can be characterized by the value $\max(a_{sr})$, with state I having $\max(a_{sr}) \approx 0.47$ and state II having $\max(a_{sr}) \approx 0.43$. In this sense, the ICs leading to state I (state II) are represented in magenta (cyan). The black and orange rectangles delimit the ICs that we use in this work to obtain each state: $(V(0), a_{sr}(0)) \in ([-20, 0], [0.40, 0.48])$, for state I and $(V(0), a_{sr}(0)) \in ([-80, -60], [0.40, 0.48])$ for II. For $g_d = 1.1415$, where state II is chaotic, the basin changes subtly, but the ICs in the rectangles still lead to their respective states.

The dynamical properties of each state can be studied using their Lyapunov exponents [35]. Table II depicts the Lyapunov spectra of the states shown in Figs. 2(a) and 2(b). The results demonstrate that for $g_d = 1.1350$ the $\max(\Lambda_I) \approx \max(\Lambda_{II}) \approx 0$, indicating two periodic states. For

TABLE II. Lyapunov spectra for IC-1 and IC-2 computed for two values of g_d .

$g_d = 1.1350$ (periodic-periodic)					
Λ_I	-0.000007	-0.001657	-0.102236	-0.197086	-5.466736
Λ_{II}	-0.000002	-0.001059	-0.122687	-0.213510	-5.420790
$g_d = 1.1415$ (periodic-chaotic)					
Λ_I	-0.000006	-0.001818	-0.099646	-0.195736	-5.471647
Λ_{II}	0.000173	-0.000017	-0.122036	-0.217536	-5.418144

$g_d = 1.1415$ the results indicate the existence of a periodic state and a chaotic one, since $\max(\Lambda_I) \approx 0$ while $\max(\Lambda_{II}) > 0$. Besides this, the most negative Lyapunov exponents indicate a difference in the linear stability of each state, thereby showing that the state I has the strongest linear stability, followed by the state II periodic, and after that by state II chaotic. The Lyapunov spectrum was evaluated using Benettin's algorithm [35,36] and including a Gram-Schmidt re-orthonormalization procedure [35]. The integration of the system is performed using a fourth-order Runge-Kutta method with fixed time-step equal to 2×10^{-2} ms to obtain the asymptotic solutions of the dynamical system after a time interval equal to 5×10^7 ms, after discarding 10^5 ms to avoid transient effects.

Multistable systems are generally extremely sensitive to perturbations [1,4,37,38]. To analyze the stability of each state, we add a current in Eq. (1), characterized by a random normal distribution with average 0 and standard deviation σ . Our results show that state II switches to state I only, and never the other way around, for the considered noise strength. Figure 3 shows the mean time that the system spends in state II before escaping to state I as a function of $1/\sigma^2$ considering a 1000 simulations. Also, it is important to emphasize that the transition from II to I is recorded when the value of a_{sr}

crosses the threshold 0.45 (see Fig. 2) and the simulations consider a maximum time of 10^8 ms. The results show that the mean time to perform a transition follows a Kramers law $\langle \tau(\sigma) \rangle \sim \exp(U/\sigma^2)$ where U corresponds to the height of the potential barrier [37,39]. In panel (a) $g_d = 1.1350$ (periodic state) $U \approx 2.2 \times 10^{-3}$. In panel (b) $g_d = 1.1415$ (chaotic state) $U \approx 2.0 \times 10^{-6}$. Based on this test, the results indicate that the chaotic state II switches more easily than the periodic state II.

III. NETWORK PROPERTIES AND SYNCHRONIZATION QUANTIFIERS

To analyze the role of bistability in synchronization, we build a neural network composed of $N = 100$ identical bursting neurons based upon the model of Braun *et al.* The evolution of the membrane potential for the i th neuron is given by

$$C_M \frac{dV_i}{dt} = -I_{i,d} - I_{i,r} - I_{i,sd} - I_{i,sr} - I_{i,l} + I_{i,syn}, \quad (7)$$

where the ionic currents are given by the Eqs. (2)–(6). The coupling scheme is characterized by electrical synapses (gap junctions), which are modeled by a generic mean-field coupling. The synaptic current is given by

$$I_{i,syn} = \frac{\varepsilon}{N} \sum_{j=1}^N (V_j - V_i) = \varepsilon(\langle V \rangle - V_i), \quad (8)$$

where ε is the coupling (synaptic) strength measured in mS/cm² which, for simplicity, is subsequently omitted. $\langle V \rangle = \frac{1}{N} \sum_{i=1}^N V_i$ is the mean-field of the network. This coupling scheme describes an all-to-all coupling, which is known to exhibit sharp transitions when the parameters are varied. This was observed in the investigation of the equilibrium of nonlinear stochastic models [40], in stochastic resonance of coupled nonlinear noisy oscillators [41], and in noise-induced bistable systems [42]. Since ε and $\langle V \rangle$ are the same for all neurons, the only difference between them is the ICs. It is worth mentioning that the results of this manuscript were reproduced for other N values (10, 1000). In these cases it is observed that smaller networks tend to synchronize faster than larger networks, but the asymptotic synchronization behavior it is not affected.

The neurons analyzed in this paper are bursting for all sets of parameters and coupling considered, such that we evaluate the burst synchronization in the network. To do this, we associate a phase θ to the neural activity of each neuron: we compute the times when the bursts start considering the minima values of $a_{i,sr}(t)$. To obtain this phase as a function of time, we linearly interpolate between the two bursting

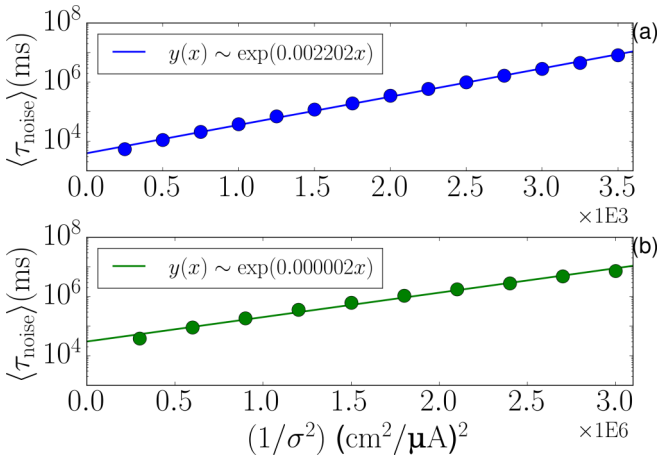


FIG. 3. Mean time that the system spends in state II before escaping to the state I, as a function of the $1/\sigma^2$ (σ is the noise strength) considering 1000 simulations and the threshold time of 10^8 ms. The slope U correspond to the height of the potential barrier of a Kramers law $\langle \tau(\sigma) \rangle \sim \exp(U/\sigma^2)$. (a) $g_d = 1.1350$ (periodic state) $U \approx 2.2 \times 10^{-3}$. (b) $g_d = 1.1415$ (chaotic state) $U \approx 2.0 \times 10^{-6}$. A transition is defined when the value of a_{sr} crosses the threshold 0.45 (see Fig. 2). No transitions from the state I to state II are observed.

events [43]:

$$\theta_i(t) = 2\pi k_i + 2\pi \frac{t - t_{k,i}}{t_{k+1,i} - t_{k,i}}, \quad t_{k,i} \leq t < t_{k+1,i}, \quad (9)$$

where $t_{k,i}$ is the time of the beginning of the k th burst of the i th neuron, the duration of this burst is $t_{k+1,i} - t_{k,i}$.

In this way, bursting synchronization can be understood as PS (phase synchronization). To quantify PS of the network, we use the Kuramoto order parameter [44]:

$$R(t) = \left| \frac{1}{N} \sum_{j=1}^N e^{i\theta_j(t)} \right|, \quad (10)$$

where $i = \sqrt{-1}$ here. In this case, $R = 1$ represents a completely phase-synchronized state, in which all neurons start their bursts at the same time. However, $R = 0$ means that each neuron in the network has a corresponding pair that is completely out-of-phase. This can correspond to a completely incoherent state (completely unsynchronized) or a state with clusters of in-phase neurons that are antiphase between themselves. If the N phases were to be randomly distributed, then the result would be $R \sim \sqrt{1/N}$ [45].

We can adapt Eq. (10) (applied to the whole network) to analyze the PS level of subgroups of the network. To do this, we evaluate the Kuramoto order parameter for each group ℓ :

$$R_\ell = \left| \frac{1}{N_\ell} \sum_{j \in \Omega_\ell} e^{i\theta_j(t)} \right|. \quad (11)$$

In this paper, we consider two groups ($\ell = 1, 2$), where each one is composed of $N_\ell = N/2$ neurons. Ω_ℓ is the set of neurons belonging to the ℓ th group, so $\Omega_1 = \{1, \dots, N/2\}$ and $\Omega_2 = \{N/2 + 1, \dots, N\}$. We also define the absolute difference between R_1 and R_2 :

$$\Delta R = |R_2 - R_1|, \quad (12)$$

to measure whether there is a difference in the synchronization states of the groups.

IV. SYNCHRONIZATION ANALYSIS AND DISCUSSIONS

To investigate the process of synchronization in a network with bistable behavior, we consider a neural network as described in Sec. III. As showed in Sec. II, the neurons depict bistable behavior as a function of sodium conductance (g_d), where both states can be reached following a set of ICs (see Fig. 2(c)). In this sense, we consider three different situations:

(i) all neurons are in the state I (periodic) with $g_d = 1.1350$ (absence of bistability);

(ii) mixture of neurons in two different states, where neurons in Ω_1 are in state I (periodic) and Ω_2 are in the state II (chaotic) with $g_d = 1.1415$;

(iii) mixture neurons in two different states, where neurons Ω_1 are in the state I (periodic) and Ω_2 are in the state II (periodic) with $g_d = 1.1350$.

The ICs for the network simulations were selected to be in a random position on the attractor of each state. To do so, an uncoupled neuron is simulated for 10^6 ms with random ICs according to the rectangles of Fig. 2(c) (for each state). Considering the last 5×10^5 ms of the simulation, a random

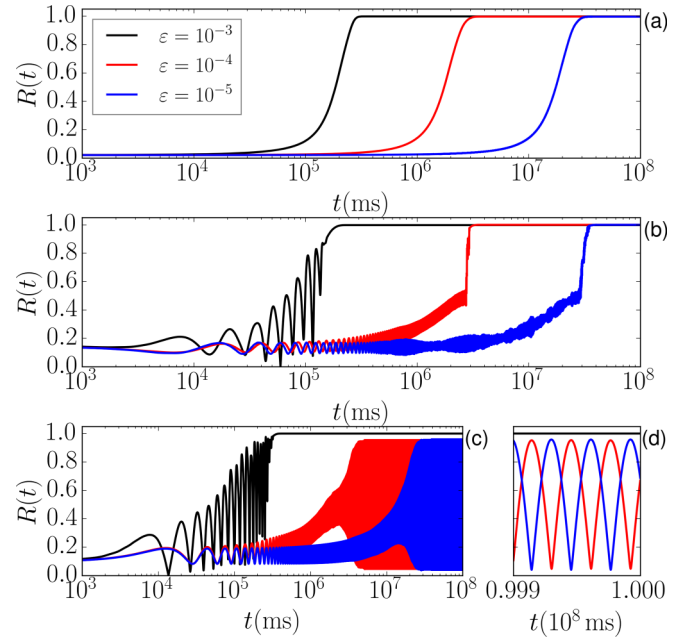


FIG. 4. Kuramoto order parameter $R(t)$ for three values of coupling $\varepsilon = 10^{-3}$ (black lines), $\varepsilon = 10^{-4}$ (red lines), and $\varepsilon = 10^{-5}$ (blue lines). Three network configurations are used: (a) a network with all neurons in state I; (b) a mixed network with half of neurons in state I (periodic) and half in state II (chaotic); (c) a mixed network with half of neurons in state I (periodic) and half in state II (periodic). (d) Magnification of the last 10^5 times of panel (c).

time instant is selected to generate the ICs for each neuron in the network. This approach allows us to initialize the network in each desired state (states I and II) avoiding any initial synchronization bias (neurons that synchronize at $t = 0$). All simulations are performed using a final time of 10^8 ms.

The evolution of the degree of PS in time is depicted in Fig. 4. We evaluate the Kuramoto order parameter as a function of time [$R(t)$] for three different values of coupling ε , 10^{-3} (black line), 10^{-4} (red line), and 10^{-5} (blue line). Figure 4(a) shows the results for case (i), where the network monotonically reaches the phase-synchronized state $R = 1$ with the time needed to reach PS decreasing as the coupling strength increases. A similar scenario is observed in Fig. 4(b), where case (ii) is used, but the transition is not monotonic as in case (i). In Fig. 4(c), showing the results for case (iii), the network only reaches PS for the higher value of coupling ($\varepsilon = 10^{-3}$). For the lower values of coupling ($\varepsilon = 10^{-4}$ and $\varepsilon = 10^{-5}$), the network does not reach a stable phase-synchronized state, but instead R oscillates between ≈ 0 and ≈ 1 . This behavior is maintained for a long period of time as observed in Fig. 4(d), which shows the last 10^5 of 10^8 (ms) of simulation.

These results indicate that bistability in the network plays an important role in its synchronization. In situation (i), PS is always reached since neurons have the same period of oscillation, so the coupling acts to simply align their phases. In cases (ii) and (iii), however, neurons have different frequencies due to being in different states. To reach PS, the coupling first needs to induce a transition in the neurons and lead them to a unique state where they have the same frequencies and

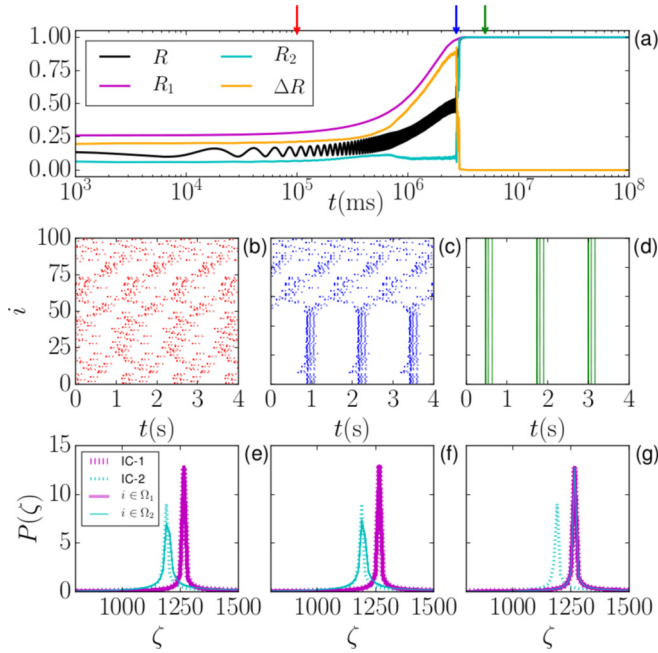


FIG. 5. Temporal evolution of the synchronization in the network at the situation (ii) with $\varepsilon = 10^{-4}$. (a) R , R_1 , R_2 , and ΔR (black, magenta, cyan, and orange lines, respectively). (b)–(d) RPs of the network where each dot corresponds to the beginning of a spike. The colored arrows indicate the times when the RPs are obtained, which match with the dots’ colors. (e)–(g) Power spectrum (based on periods ζ) of neurons (same context of panels (b)–(d), respectively), where the magenta (cyan) dashed line represents the isolated neuron initialized with IC-1 (IC-2), while the magenta (cyan) solid lines represent the neurons in the group Ω_1 (Ω_2).

only then it can align their phases. The details behind these processes are analyzed in the next sections.

A. Mixed states (periodic-chaotic)

In this section we consider a network composed of $N/2$ neurons in state I (periodic) and $N/2$ neurons in the state II (chaotic), where $g_d = 1.1415$. The transition to PS in this case is similar for the three values of coupling strength, so we use the representative situation for $\varepsilon = 10^{-4}$. The results are depicted in Fig. 5, where the black line in Fig. 5(a) corresponds to R , the magenta and cyan lines represent the local order parameters R_1 and R_2 , respectively, and the orange line presents ΔR . In this case, the network as a whole starts nonsynchronized. As the system evolves in time, R_1 increases slowly while R_2 remains at $R_2 \approx 0$, leading to a local maximum of ΔR . The first group then reaches PS, $R_1 = 1$, closely followed by the second one, whose R_2 quickly rises to 1 indicating that the second group reaches PS after the first one. In this case, the global PS behavior is also reached ($R = 1$).

We then select three time instants denoted by the colored arrows above Fig. 5(a) to analyze the spatiotemporal patterns of the network. Figures 5(b)–5(d) depict the raster plots (RPs) where each dot corresponds to the beginning of a spike for each neuron, marked when $V_i(t) > -20$ mV (with a positive derivative). Figure 5(b) shows the RP for a nonsynchronized state of the network. An interesting behavior

is observed in Fig. 5(c), where the first group is synchronized ($R_1 \approx 1$) while the second one does not ($R_2 \approx 0$). This behavior is typical of chimera states, where the system can display the coexistence of one coherent-phase-locked group with an incoherent-nonsynchronized one [46]. In this case, the chimera is transient [47,48] and disappears when the second group gains synchronization, shown in Fig. 5(d), where the network as a whole is synchronized. Furthermore, Figs. 5(e)–5(g) show the power spectrum of the neurons, given by the fast Fourier transform of $V(t)$ as function of the period ζ . Here, the magenta (cyan) dashed line represents the isolated neuron initialized with IC-1 (IC-2)—state I (state II), while the magenta (cyan) solid lines represent the neurons of Ω_1 (Ω_2). It has to be noted that the cyan dashed line represents a chaotic state, as seen in the inner panel of Fig. 2(b), but its chaoticity is too weak to be detected in the Fourier transform. In Figs. 5(e) and 5(f), the neurons remain close to the initial states, and the network is not synchronized, while in Fig. 5(g), the neurons initialized in state II already made the transition to state I and the entire network is completely synchronized.

B. Mixed states (periodic-periodic)

In this section we consider a network composed of $N/2$ neurons in state I (periodic) and $N/2$ neurons in the state II (periodic), where $g_d = 1.1350$. In this case, if the coupling strength is not strong enough, the network does not synchronize as a whole. To analyze this situation, we set $\varepsilon = 10^{-4}$ [red line of Figs. 4(c) and 4(d)]. Figure 6(a) depicts the synchronization features of the network such that R , R_1 , R_2 , and ΔR are represented by the black, magenta, cyan, and orange lines, respectively. The network starts in the nonsynchronized state ($R \approx 0$) and, as time evolves, the R oscillates with increasing amplitude. At the group level, however, we observe that R_1 increases more quickly than R_2 , leading to a local maximum of ΔR . After that, R_2 also increases, leading both R_1 and R_2 close to 1, but $R_1 > R_2$. Figure 6(b) depicts the last 10^5 ms of the simulation, suggesting a beating process of R .

To understand this behavior, we select four time instants of the simulation, represented by the colored arrows above Figs. 6(a) and 6(b). Figures 6(c)–6(f) represent the RPs corresponding to the color of the arrow. First, an incoherent behavior is observed in the red dots [Fig. 6(c)]. As time evolves, the network depicts a transient chimera state, as observed by the blue dots [Fig. 6(d)]. Eventually, each group depicts PS separately, since R_1 and R_2 show values close to one. However, each group evolves following its own frequency, which leads to momentary phase-synchronized and phase-nonsynchronized states in the entire network (the oscillatory behavior of R). The green dots in Fig. 6(e) and gray dots in Fig. 6(f) show clearly this behavior, where an antiphase behavior of the groups and a PS for the entire network can be observed, respectively. It has to be noted that the first group depicts higher synchronization levels than the second group $R_1 > R_2$, this asymmetry in the network occurs due to the coupling not being strong enough to completely synchronize the second state. Figures 6(g) and 6(h) show the power spectrum of the neurons considering the same context than Figs. 6(e) and 6(f), respectively. We observe that in both cases there is no transition and the neurons in each group (solid lines)

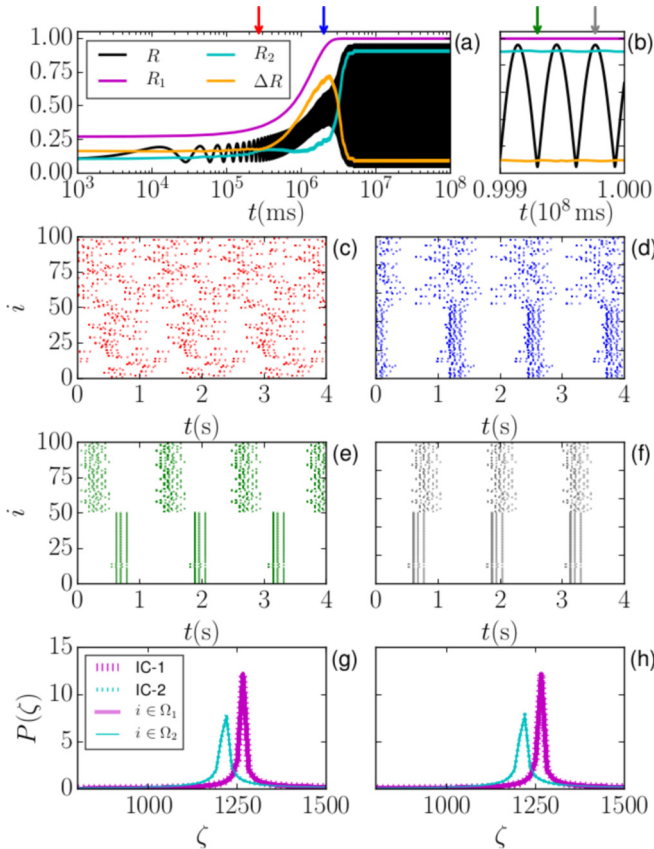


FIG. 6. Detailed analysis in the synchronization of situation (iii) with $\varepsilon = 10^{-4}$. (a) R , R_1 , R_2 , and ΔR (black, magenta, cyan, and orange lines) as a function of time are depicted in. (b) Last 10^5 ms of the simulation, where an oscillatory behavior of R is evidenced while each group assumes PS separately. (c)–(f) RPs obtained for the network in the times indicated by the colored arrows. (g), (h) Power spectrum of the neurons—considering the situations of panels (e), (f).

remain close to their initial states (dashed lines), which are represented by in magenta (state I) and cyan (state II).

Figure 7(a) represents the detailed analysis of synchronization for a stronger coupling value, $\varepsilon = 10^{-3}$. The color scheme here follows the same one of the previous figure. In this case, the network also starts in a nonsynchronized case and R gains amplitude reaching the phase synchronized asymptotic state ($R = 1$) as time evolves. Both groups now depict the same phase synchronized state at the end of the simulation. However, the transition to PS shows an interesting dynamics: while group 1 approaches monotonically the state of PS, the second one approaches in an oscillatory manner. In addition, for $t \sim 2 \times 10^5$ ms, the second group momentarily loses synchronization and a peak can be observed in $\Delta R \approx 0.9$.

We select three time instants represented by the colored arrows to evaluate the RPs. Figure 7(b) depicts the nonsynchronized case. Figure 7(c) depicts the RP for the network in the time instant where the second group loses synchronization and ΔR assumes a maximum characterizing a transient chimera state [47]. This behavior occurs for a short period of time. Figure 7(d) shows the RP for the network when PS

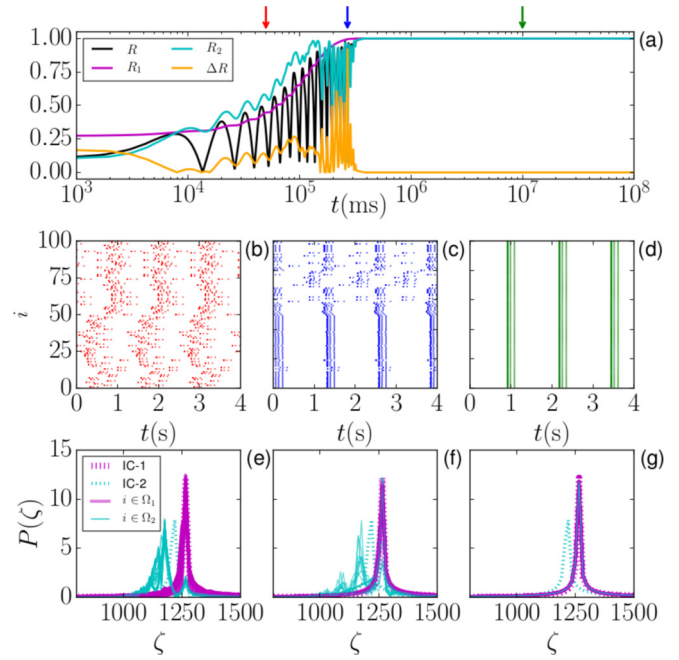


FIG. 7. Detailed analysis in the synchronization of situation (iii) with $\varepsilon = 10^{-3}$. (a) R , R_1 , R_2 , and ΔR (black, magenta, cyan, and orange lines) as a function of time. (b)–(d) RPs for the network where the dots’ colors match the arrows’ colors, which indicate the analyzed times. (e)–(g) Power spectrum of the neurons (same situation than panels (b)–(d), respectively).

is reached and maintained until the end of the simulation. Figures 7(e)–7(g) show the power spectrum of the neurons (considering the same situation than Figs. 7(b)–7(d), respectively). Here, as used before, the magenta (cyan) dashed line represents the isolated neuron initialized with IC-1 (IC-2), while the magenta (cyan) solid lines represent the neurons of Ω_1 (Ω_2). Concerning Fig. 7(e) we note that the coupling is strong enough to initially disturb the states to a new state with slightly different frequencies from the initial states. In Fig. 7(f), after the evolution of some pseudo-periods, there is a partial transition to the state I. At last, in Fig. 7(g), all neurons transition to state I and a complete synchronization is obtained.

As indicated previously, the characteristics of the transition to PS vary with the coupling strength ε . To study this further, 100 different simulations are performed with different ICs and Fig. 8(a) shows the number of these simulations \mathcal{N} in which all neurons initialized in state II transition to state I and the entire network reaches PS. For $\varepsilon < 0.00014$ this is zero, which means that no transition is observed during the simulation of 10^8 ms. For $0.00014 \leq \varepsilon < 0.00030$, only for a fraction of the simulations ($0 < \mathcal{N} < 100$) the network reaches PS and, for $\varepsilon \geq 0.00030$ in all simulations the neurons’ transitions to state I are observed. Figure 8(b) depicts the time when the last neuron initialized in state II transitions to state I, named τ_{last} . In this case, the higher the coupling the smaller the time at which this happens.

The results so far considering a network composed of neurons in two different periodic states indicate a very interesting region of coupling strength in which the final state

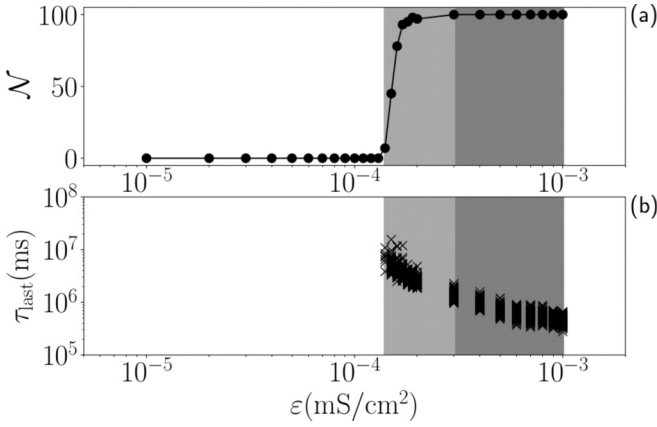


FIG. 8. (a) Number of simulations where the network depicts PS, meaning all neurons transition to state I, as a function of ϵ . For $\epsilon < 0.00014$, no transitions are observed. For $0.00014 < \epsilon < 0.00030$ (light-gray area), a fraction of simulations (ICs) induce the network to present PS, and, at last, for $\epsilon > 0.00030$ (dark-gray area), the network depicts PS for all simulations (ICs). (b) Time when the last neuron transitions to state I (τ_{last}) as a function of ϵ . Here, 100 simulations with different ICs are performed.

of synchronization of the network depends on the ICs of the system. In this way, setting $\epsilon = 0.00016$ (light-gray area), we analyze a special case whose results are depicted in Fig. 9. Figure 9(a) depicts the time evolution of R , and Fig. 9(b) depicts the number of neurons in each state $n_1(t)$ and $n_2(t)$. For this IC, there is a partial transition where a part of the neurons transition to state I. In this case, R oscillates between 0.0 and 1.0 as t evolves, but after a certain time the oscillation becomes restricted between 0.5 and 1.0. We then set the time

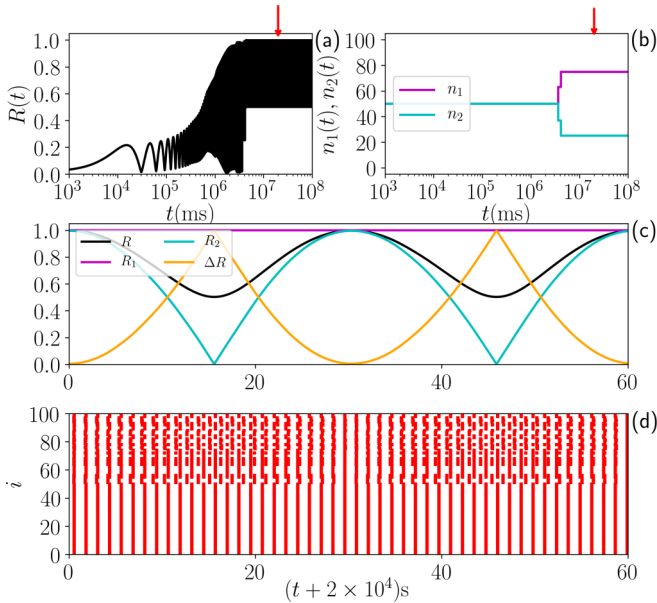


FIG. 9. (a) Time evolution of $R(t)$ using $\epsilon = 1.6 \times 10^{-4}$. (b) The number of neurons in each state. We selected one IC where a partial transition from state II to state I is observed. (c) Synchronization features of the network considering the time region indicated by the red arrow. (d) RP of the network (bursts only) for the same condition.

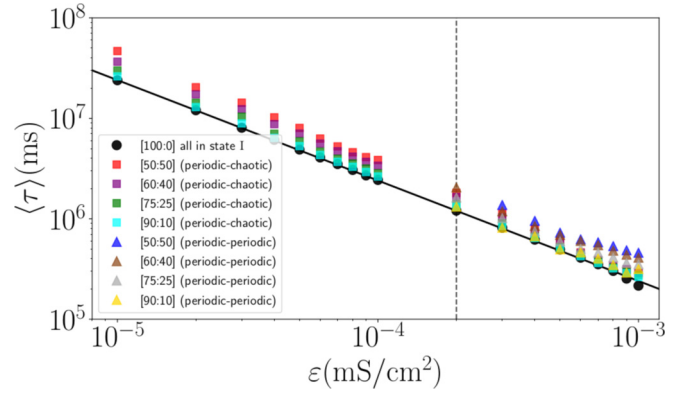


FIG. 10. Mean characteristic time (τ) needed for the network to reach PS as a function of ϵ for 100 ICs, initializing the network in different configurations of states $[n_1(0) : n_2(0)]$. The black dots correspond to all neurons in state I [situation (i)], following a power-law curve (solid black line) $f(\epsilon) \sim \epsilon^{-1}$. The squares represent configurations where state II is chaotic, in red [50:50] [situation (ii)], purple [60:40], green [75:25], and cyan [90:10]. For the triangles, state II is periodic, in blue [50:50] [situation (iii)], brown [60:40], gray [75:25], and yellow [90:10]. The dashed line delimits the critical value (ϵ^*), where for $\epsilon < \epsilon^*$ no transitions are observed.

region (red arrow) to analyze the PS and the spatiotemporal of the network. Figure 9(c) shows R , R_1 , R_2 , and ΔR , where we observe that the first group is on a state of PS while R_2 oscillates between 0.0 and 1.0. The RP of the network (bursts only), depicted in Fig. 9(d), shows a coexistence of two frequencies in the second group, explaining the oscillations in R_2 . This behavior generates a beating process, making the R oscillates. In this situation, chimera states occur: they appear when the second group is nonsynchronized, then disappear when it synchronizes and reappear later again.

For a better understanding about the role of bistability in the synchronization process, we show the mean time to reach a synchronized state ($R \geq 0.99$) (τ) as a function of ϵ (Fig. 10) considering 100 ICs. Different network configurations are considered, varying the number of neurons initialized in each state $[n_1(0), n_2(0)]$. The black dots correspond to the situation (i) (all neurons in state I) where the mean time decays with a power-law $f(\epsilon) \sim \epsilon^{-1}$. The squares represent configurations where state I is periodic and state II is chaotic, in red [50:50] [situation (ii)], purple [60:40], green [75:25], and cyan [90:10]. For triangles, both states are periodic, in blue [50:50] [situation (iii)], brown [60:40], gray [75:25], and yellow [90:10]. As shown before, for this case the coupling must be sufficiently strong for the network to reach PS, so for coupling values lower than a critical value (dashed line) no transition is observed and no triangles are seen. At last, on average the time to reach PS decays as the coupling increases for all cases and the higher the number of neurons in state I the closer to the situation (i).

V. CONCLUSIONS

Throughout this paper, we have analyzed the effects of bistability on the synchronization process of neural networks. We have shown that a neuron simulated through a Hodgkin-Huxley-type model depicts bistability. As the

sodium conductance is varied, one of the states, named state I always depicts a periodic behavior. The other state, named state II, suffers a sequence of period-doubling bifurcations from periodic to chaotic behavior. In this scenario, we have analyzed the stability of these states by evaluating the Lyapunov spectrum and also with noise application. We have found that state I is more stable than state II and also that state II periodic is more stable than state II chaotic.

We have simulated a network of identical neurons coupled by electrical synapses modeled by mean-field coupling. We have considered three network configurations: (i) all neurons in state I; (ii) half of the network in state I and half in state II (chaotic); (iii) half of the network in state I and half in state II (periodic). We have shown that in case (i) and (ii) the network always reaches PS (phase synchronization), but the time to do that increases as the coupling strength decreases. Also, on average, this time is always greater in case (ii), denouncing a delay generated by the bistability. In case (iii), small coupling does not lead the network to PS, and each part of the network synchronizes in different frequencies. For higher coupling values, the network reaches PS but always taking longer times than the other cases. During the transition to PS, configurations (ii) and (iii) depict chimera states, in which part of the network is phase synchronized and the other part is not.

The process of PS in cases (ii) and (iii) is only possible due to the transitions that occur from state II (periodic or chaotic) to state I (periodic). These transitions are essential for PS since all neurons have to be in the same state (i.e., have the same frequency). In addition, we have analyzed the synchronization process in case (iii) and have shown that the ICs for the neurons are very important to the synchronization features of the network. We have found an intermediary region of coupling strength where different ICs lead the network to different behaviors: no neuron transitions; all neurons transition from

state II to state I; only part of the neurons transition. At last, we have considered different fractions of neurons in each state and have found that, on average, the time the network takes to reach PS decreases as the coupling strength increases and the behavior gets closer to configuration (i) as the fraction of neuron in state I increases.

In summary, bistability plays an important role in the synchronization of neural networks. The simple existence of two distinct stable states can lead the network to different states of synchronization, depending on the initialization of the system: from completely phase synchronized to completely antiphase synchronized. This dependence on the initialization is very strong, so slightly different network states can eventually lead to largely different states of synchronization. Furthermore, extensive simulations (not shown) have revealed that these phenomena still occur in the presence of weak noise or small parameter heterogeneity. Otherwise, strong noise or large parameter heterogeneity destroy these behaviors. Bistability also leads to the existence of a variety of chimera states. These synchronization and chimera states occur due to the difference in the stability of the states of the uncoupled neurons, thus highlighting the importance of the individual neuronal dynamics [27].

ACKNOWLEDGMENTS

This study was financed in part by the Coordenação de Aperfeiçoamento de Pessoal de Nível Superior, Brasil (CAPES), Finance Code 001. The authors also acknowledge the support of Conselho Nacional de Desenvolvimento Científico e Tecnológico, CNPq, Brazil, Grants No. 302785/2017-5, No. 308621/2019-0, No. 304918/2017-2, No. 424803/2018-6, and No. 310228/2020-4, and Financiadora de Estudos e Projetos (FINEP). Computer simulations were performed at the LCPAD cluster at Universidade Federal do Paraná, supported by FINEP (CT-INFRA).

-
- [1] U. Feudel, *Int. J. Bifurcat. Chaos* **18**, 1607 (2008).
 - [2] E. Ott, *Chaos in Dynamical Systems* (Cambridge University Press, Cambridge, UK, 2002).
 - [3] S. H. Strogatz, *Nonlinear Dynamics and Chaos with Student Solutions Manual: With Applications to Physics, Biology, Chemistry, and Engineering* (CRC Press, Boca Raton, FL, 2018).
 - [4] A. N. Pisarchik and U. Feudel, *Phys. Rep.* **540**, 167 (2014).
 - [5] F. T. Arecchi, R. Meucci, G. Puccioni, and J. Tredicce, *Phys. Rev. Lett.* **49**, 1217 (1982).
 - [6] N. Ganapathisubramanian and K. Showalter, *J. Chem. Phys.* **80**, 4177 (1984).
 - [7] D. Paillard, *Nature (London)* **391**, 378 (1998).
 - [8] J. A. Hertz, *Introduction to the Theory of Neural Computation* (CRC Press, Boca Raton, FL, 2018).
 - [9] C. C. Canavier, D. A. Baxter, J. W. Clark, and J. H. Byrne, *J. Neurophysiol.* **69**, 2252 (1993).
 - [10] J. Foss, A. Longtin, B. Mensour, and J. Milton, *Phys. Rev. Lett.* **76**, 708 (1996).
 - [11] M. Sainz-Trapaga, C. Masoller, H. A. Braun, and M. T. Huber, *Phys. Rev. E* **70**, 031904 (2004).
 - [12] J. Ma and J. Wu, *Neural Comput.* **19**, 2124 (2007).
 - [13] E. R. Kandel, J. H. Schwartz, T. M. Jessell, S. A. Siegelbaum, and A. J. Hudspeth, *Principles of Neural Science*, Vol. 4 (McGraw-Hill, New York, 2000).
 - [14] F. Mormann, K. Lehnertz, P. David, and C. E. Elger, *Physica D* **144**, 358 (2000).
 - [15] C. Hammond, H. Bergman, and P. Brown, *Trends Neurosci.* **30**, 357 (2007).
 - [16] O. V. Popovych and P. A. Tass, *Front. Neurol.* **5**, 268 (2014).
 - [17] I. Dinstein, K. Pierce, L. Eyster, S. Solso, R. Malach, M. Behrmann, and E. Courchesne, *Neuron* **70**, 1218 (2011).
 - [18] M. D. Greicius, G. Srivastava, A. L. Reiss, and V. Menon, *Proc. Natl. Acad. Sci. USA* **101**, 4637 (2004).
 - [19] H. A. Braun, M. Dewald, K. Schäfer, K. Voigt, X. Pei, K. Dolan, and F. Moss, *J. Comput. Neurosci.* **7**, 17 (1999).
 - [20] H. A. Braun, M. T. Huber, M. Dewald, K. Schäfer, and K. Voigt, *Int. J. Bifurcat. Chaos* **8**, 881 (1998).
 - [21] U. Feudel, A. Neiman, X. Pei, W. Wojtenek, H. A. Braun, M. Huber, and F. Moss, *Chaos* **10**, 231 (2000).
 - [22] A. L. Hodgkin and A. F. Huxley, *J. Physiol.* **117**, 500 (1952).
 - [23] M. Burek, R. Follmann, and E. Rosa, *Biosystems* **180**, 1 (2019).
 - [24] B. R. R. Boaretto, R. C. Budzinski, T. L. Prado, J. Kurths, and S. R. Lopes, *Chaos* **28**, 106304 (2018).

- [25] R. C. Budzinski, B. R. R. Boaretto, T. L. Prado, and S. R. Lopes, *Chaos, Solitons Fractals* **123**, 35 (2019).
- [26] B. R. R. Boaretto, R. C. Budzinski, T. L. Prado, J. Kurths, and S. R. Lopes, *Physica A* **497**, 126 (2018).
- [27] B. R. R. Boaretto, C. Manchein, T. L. Prado, and S. R. Lopes, *Neural Netw.* **137**, 97 (2021).
- [28] R. C. Budzinski, B. R. R. Boaretto, T. L. Prado, and S. R. Lopes, *Phys. Rev. E* **96**, 012320 (2017).
- [29] T. A. Glaze, S. Lewis, and S. Bahar, *Chaos* **26**, 083119 (2016).
- [30] S. Postnova, C. Finke, W. Jin, H. Schneider, and H. A. Braun, *J. Physiol.-Paris* **104**, 176 (2010).
- [31] C. Finke, J. A. Freund, E. Rosa Jr, P. H. Bryant, H. A. Braun, and U. Feudel, *Chaos* **21**, 047510 (2011).
- [32] P. R. Shorten and D. J. N. Wall, *Bull. Math. Biol.* **62**, 695 (2000).
- [33] W. Löscher and D. Schmidt, *Epilepsy Res.* **50**, 3 (2002).
- [34] W. Löscher, H. Klitgaard, R. E. Twyman, and D. Schmidt, *Nature Rev. Drug Discov.* **12**, 757 (2013).
- [35] A. Wolf, J. B. Swift, H. L. Swinney, and J. A. Vastano, *Physica D* **16**, 285 (1985).
- [36] G. Benettin, L. Galgani, A. Giorgilli, and J.-M. Strelcyn, *Meccanica* **15**, 9 (1980).
- [37] S. Kraut, U. Feudel, and C. Grebogi, *Phys. Rev. E* **59**, 5253 (1999).
- [38] P. R. Sharma, M. D. Shrimali, A. Prasad, and U. Feudel, *Phys. Lett. A* **377**, 2329 (2013).
- [39] P. Hänggi, P. Talkner, and M. Borkovec, *Rev. Mod. Phys.* **62**, 251 (1990).
- [40] R. C. Desai and R. Zwanzig, *J. Stat. Phys.* **19**, 1 (1978).
- [41] A. Pikovsky, A. Zaikin, and M. A. de la Casa, *Phys. Rev. Lett.* **88**, 050601 (2002).
- [42] R. Kawai, X. Sailer, L. Schimansky-Geier, and C. Van den Broeck, *Phys. Rev. E* **69**, 051104 (2004).
- [43] S. Boccaletti, J. Kurths, G. Osipov, D. Valladares, and C. Zhou, *Phys. Rep.* **366**, 1 (2002).
- [44] Y. Kuramoto, *Prog. Theor. Phys. Suppl.* **79**, 223 (1984).
- [45] A. Arenas, A. Díaz-Guilera, J. Kurths, Y. Moreno, and C. Zhou, *Phys. Rep.* **469**, 93 (2008).
- [46] D. M. Abrams and S. H. Strogatz, *Phys. Rev. Lett.* **93**, 174102 (2004).
- [47] A. Zakharova, M. Kapeller, and E. Schöll, *Phys. Rev. Lett.* **112**, 154101 (2014).
- [48] F. P. Kemeth, S. W. Haugland, L. Schmidt, I. G. Kevrekidis, and K. Krischer, *Chaos* **26**, 094815 (2016).